Chemical Science

EDGE ARTICLE

View Article Online
View Journal | View Issue

Cite this: *Chem. Sci.*, 2018, **9**, 3767

Self-complementary nickel halides enable multifaceted comparisons of intermolecular halogen bonds: fluoride ligands *vs.* other halides†‡

Vargini Thangavadivale,§[a] Pedro M. Aguiar,[ab] Naseralla A. Jasim,[a] Sarah J. Pike,¶[a] Dan A. Smith,§[a] Adrian C. Whitwood,*[a] Lee Brammer*[c] and Robin N. Perutz*[a]

The syntheses of three series of complexes designed with self-complementary motifs for formation of halogen bonds between an iodotetrafluorophenyl ligand and a halide ligand at square-planar nickel are reported, allowing structural comparisons of halogen bonding between all four halides $C_6F_4I\cdots X–Ni$ (X = F, Cl, Br, I). In the series *trans*-[NiX(2,3,5,6-C_6F_4I)(PEt_3)$_2$] **1pX** and *trans*-[NiX(2,3,4,5-C_6F_4I)(PEt_3)$_2$] (X = F, Cl, Br, I) **1oX**, the iodine substituent on the benzene ring was positioned *para* and *ortho* to the metal, respectively. The phosphine substituents were varied in the series, *trans*-[NiX(2,3,5,6-C_6F_4I)(PEt_2Ph)$_2$] (X = F, I) **2pX**. Crystal structures were obtained for the complete series **1pX**, and for **1oF**, **1oCl**, **1oI** and **2pI**. All these complexes exhibited halogen bonds in the solid state, of which **1pF** exhibited unique characteristics with a linear chain, the shortest halogen bond $d(C_6F_4I\cdots F–Ni)$ = 2.655(5) Å and the greatest reduction in halogen bond distance (I···F) compared to the sum of the Bondi van der Waals radii, 23%. The remaining complexes form zig-zag chains of halogen bonds with distances also reduced with respect to the sum of the van der Waals radii. The magnitude of the reductions follow the pattern F > Cl ∼ Br > I, **1pX** > **1oX**, consistent with the halogen bond strength following the same order. The variation in the I···X–Ni angles is consistent with the anisotropic charge distribution of the halide ligand. The temperature dependence of the X-ray structure of **1pF** revealed a reduction in halogen bond distance of 0.055(7) Å on cooling from 240 to 111 K. Comparison of three polymorphs of **1oI** shows that the halogen bond geometry may be altered significantly by the crystalline environment. The effect of the halogen bond on the ^{19}F NMR chemical shift in the solid state is demonstrated by comparison of the magic-angle spinning NMR spectra of **1pF** and **1oF** with that of a complex incapable of halogen bond formation, *trans*-[NiF(C_6F_5)(PEt_3)$_2$] **3F**. Halogen bonding causes deshielding of δ_{iso} in the component of the tensor perpendicular to the nickel coordination plane. The results demonstrate the potential of fluoride ligands for formation of halogen bonds in supramolecular structures.

Received 23rd February 2018
Accepted 19th March 2018

DOI: 10.1039/c8sc00890f

rsc.li/chemical-science

Introduction

Metal fluoride complexes should provide the strongest halogen bond acceptors among metal halide complexes. Their halogen bonding ability has been addressed in solution, but supramolecular structures connecting metal fluoride complexes *via* halogen bonds are unknown according to a current crystallographic database search. This study reveals that they are indeed capable of forming halogen-bonded chains and allows comparisons of their structures to those of corresponding metal chlorides, bromides and iodides.

Halogen bonding (XB) interactions between the electropositive region of a covalently-bound halogen and a Lewis base are increasingly recognised as motifs in secondary bonding that bear comparison with hydrogen bonds.[1–5] They have been utilized in solution,[4,6,7] for example for anion recognition,[4,8] in catalysis,[9] in medicinal chemistry,[10] in biological systems including proteins and nucleic acid junctions,[6,7,11–14] in liquid crystals[15] and especially in supramolecular chemistry[8] and crystal engineering,[16,17] where halogen bonding can provide suitable motifs for self-assembly of molecules. The halogen bond is most commonly described as an electrostatically attractive interaction between a σ-hole generated

[a]*Department of Chemistry, University of York, York YO10 5DD, UK. E-mail: adrian.whitwood@york.ac.uk; robin.perutz@york.ac.uk*

[b]*Département de Chimie, l'Université de Montréal, Montréal, QC H3C 3J7, Canada*

[c]*Department of Chemistry, University of Sheffield, Sheffield S3 7HF, UK. E-mail: lee.brammer@sheffield.ac.uk*

† Experimental datasets associated with this paper were deposited with the University of York library.

‡ Electronic supplementary information (ESI) available. CCDC 1825404, 1825439–1825452. For ESI and crystallographic data in CIF or other electronic format see DOI: 10.1039/c8sc00890f

§ Present addresses: CatScI Ltd, CBTC2, Capital Business Park, Wentloog, Cardiff, CF3 2PX, UK.

¶ Present addresses: School of Chemistry and Bioscience, Richmond Road, University of Bradford, Bradford, BD1 1DP, UK.

on a covalently-bound halogen, archetypally iodine in an organo-iodine compound containing fluorine substituents, and a Lewis base.[18–20] The organo-iodine compound is described as the halogen-bond donor and the base as the halogen-bond acceptor.

Halogen bonding interactions involving metal complexes in the solid state have been demonstrated extensively.[16,21–34] Three approaches to investigating such interactions have been adopted, the design of self-complementary molecules,[30,34] co-crystallization of the halogen-bond donor with the halogen-bond acceptor[31] or formation of halogen bonds between ion-pairs.[21,29,32,33] In a self-complementary molecule, the halogen-bond acceptor and the donor are both present in the same molecule. A series of such complexes exhibiting C–X···X′–M (M = Pt, Pd, X = Cl, Br, I; X′ = Cl, Br) halogen bonds was demonstrated by use of halopyridine ligands as the XB donors and halide ligands as the XB acceptors.[30,34] Among examples of halogen-bonded co-crystals is a series of pincer palladium halides PdX(PCP) (PCP = 2,6-bis[(di-*tert*-butylphosphino) methyl]phenyl; X = Br, Cl and I) co-crystallized with I_2, 1,4-$C_6F_4I_2$ and $I(CF_2)_4I$ as XB donors.[31] The metal–halide complexes showed the general trend of the strength of the C–I···X–Pd halogen-bonding interaction decreasing in the order X = Cl > Br > I, and of the three XB donors used, I_2 showed the strongest interaction.[31] These halogen-bond interactions emphasize the different roles of the two halogens involved in C–X···X′–M interactions. The carbon-bound halogen serves the Lewis acidic role and adopts an approximately linear C–X···X′ interaction geometry, whereas the metal-bound halogen serves in a Lewis basic role and adopts a markedly bent X···X′–M geometry. These geometries maximize the interaction between the positive potential of the organic halogen and the most negative region of the inorganic halogen. A different class of co-crystals is illustrated by ruthenium halide complexes that form a halogen-bonded network with dihalogens (Br_2 or I_2).[35] In spite of these thorough studies, the behaviour of metal fluorides with respect to halogen bonding remains unknown in the crystalline state.

We have reported the hydrogen- and halogen-bonding properties of group 10 metal fluoride complexes in solution for complexes of the type *trans*-[MF(Ar^F)(PR_3)$_2$] (M = Ni, Pd, Pt, Ar^F = tetrafluoropyridyl and related fluoropyridyls, R = Et, Cy).[36–38] Measurement of the dependence of the chemical shift of the ^{19}F NMR resonance of the metal fluoride moiety on the concentration of added iodopentafluorobenzene demonstrated the formation of the F_5C_6–I···F–Ni halogen bonds (Scheme 1a) and allowed us to determine their free energies and enthalpies of formation, and in so doing to establish metal–fluorides as among the strongest halogen bond acceptors. This conclusion is supported by related work showing that zinc and magnesium fluoride complexes behave analogously.[39,40]

We have attempted to co-crystallize the nickel fluoride complexes with halogen-bond donors in order to determine the geometry of the halogen bond but without success. We turned instead to the alternative strategy, design of self-complementary molecules. The feasibility of this approach is indicated by the crystallization of *trans*-[NiF{$C_5NF_3(NH_2)$}(PEt_3)$_2$] which shows a hydrogen bond between the amino group on the fluoropyridyl ligand and the nickel fluoride on the adjacent molecule.[37] We

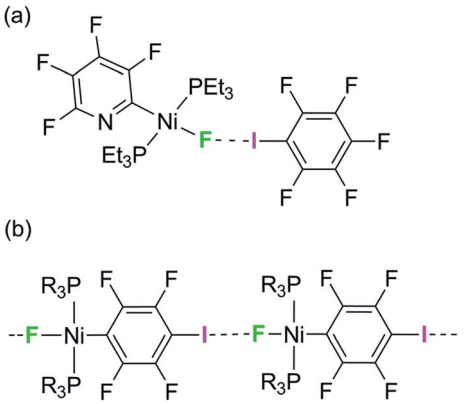

Scheme 1 (a) Formation of halogen bonds with nickel fluoride in solution and (b) structural motif with envisaged intermolecular halogen-bonding interaction.

therefore set about the synthesis of a nickel fluoride complex with an iodine substituent on a fluorophenyl ligand, which would enable formation of an intermolecular halogen-bond network (Scheme 1b) between the iodine as halogen-bond donor and the nickel-fluoride as halogen-bond acceptor. We report the synthesis and structures of a series of Ni–X complexes (X = F, Cl, Br, I) with the halide ligand as halogen-bond acceptors, iodine at the 2- or 4-position on the tetrafluorophenyl ligand as halogen-bond donor and different phosphine groups. Their crystal structures reveal the changes in geometry and strength of the halogen-bonding interaction in the solid state. Geometric trends are determined as a function of halogen, regiochemistry, influence of crystalline environment and temperature. For examples with fluoride ligands (X = F) we also show that the chemical shift tensor in the ^{19}F MAS NMR spectra is highly sensitive to halogen bond formation and strength.

Results

Complexes of the type illustrated in Scheme 1b were accessed by reaction of Ni(COD)$_2$ with 2 equiv. of trialkylphosphine[41] to form Ni(COD)(PEt_3)$_2$ followed by reaction with 1,4-diiodo-2,3,5,6-tetrafluorobenzene or 1,2-diiodo-3,4,5,6-tetrafluorobenzene. This synthetic method is similar to that used by Bennett with 1,6-dibromo-2,3,4,5-tetrafluorobenzene.[42] Oxidative addition of one of the carbon-iodine bonds of diiodotetrafluorobenzene gives rise to a nickel–iodide complex that may then be converted into a nickel fluoride, chloride or bromide. The resulting complexes contain a coordinated C_6F_4I ligand as a halogen bond donor and the nickel halide as a halogen-bond acceptor. The complexes and their labels are shown in Scheme 2. The labels **1pX** and **1oX** refer to the position of the iodine substituent on the ring, either *para* (*p*) or *ortho* (*o*) to nickel, and the halogen (X) bound directly to nickel.

Synthesis and characterization of *trans*-[NiX(2,3,5,6-C_6F_4I)(PEt_3)$_2$], 1pX (X = I, F, Cl, Br)

The synthetic methods for the **1pX** series are shown in Scheme 3. The initial reaction with 1,4-diiodo-2,3,5,6-tetrafluorobenzene resulted in red *trans*-[NiI(2,3,5,6-

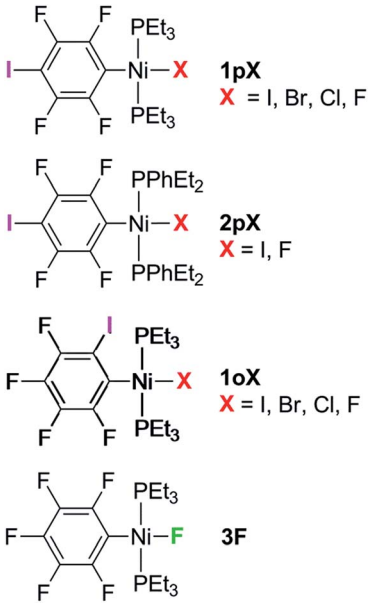

Scheme 2 Key to complexes.

$C_6F_4I)(PEt_3)_2]$ **1pI** as the major product in 84% yield. The $^{31}P\{^1H\}$-NMR spectrum showed a singlet at δ 15.4 for the two phosphorus atoms in equivalent environments, consistent with a *trans* geometry. The fluorine atoms of the aromatic ring of **1pI** appeared in the ^{19}F-NMR spectrum as two second-order multiplets, AA′XX′ at δ −113.3 and δ −123.6, resulting from the coupling of the neighbouring magnetically inequivalent *ortho* and *para* fluorine atoms on the ring. The peak at *m*/*z* 695.93 (due to ^{58}Ni with corresponding peaks for other nickel isotopes) in the LIFDI mass spectrum was identified as the molecular ion $[M]^+$ base peak (100%) of *trans*-$[NiI(2,3,5,6\text{-}C_6F_4I)(PEt_3)_2]$. In addition, the $^{31}P\{^1H\}$-NMR and ^{19}F-NMR spectra showed singlets at δ 13.5 and δ −117.7, respectively, due to a minor product. The identity of this species as $[trans\text{-}NiI(PEt_3)_2]_2(\mu\text{-}2,3,5,6\text{-}C_6F_4)$ was demonstrated by the peak at 990.17 in the LIFDI mass spectrum which corresponds to the molecular ion $[M]^+$. This complex arises from the oxidative addition of both the iodine atoms on the 1,4-diiodotetrafluorobenzene (Scheme 4).

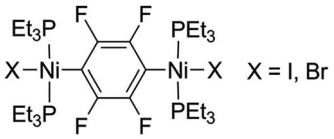

Scheme 4 Dinuclear product $[trans\text{-}NiX(PEt_3)_2]_2(\mu\text{-}2,3,5,6\text{-}C_6F_4)$.

The reaction of **1pI** with $[NMe_4]F$ in THF gave a colour change from red to yellow in 5 h at room temperature. After purification and removal of unreacted **1pI**, a yellow solid was isolated in 71% yield. The major product of the reaction was identified as *trans*-$[NiF(2,3,5,6\text{-}C_6F_4I)(PEt_3)_2]$ **1pF**. The $^{31}P\{^1H\}$-NMR spectrum showed a resonance at δ 13.1 as a doublet with $^2J_{PF} = 46$ Hz.[41] The ^{19}F-NMR spectrum of the purified product showed two resonances at δ −113.8 and δ −124.9 for the four aromatic fluorine atoms with second-order multiplets AA′XX′ spin system. The nickel fluoride resonance of the complex was observed as a triplet at δ −387.9, $J_{PF} = 46$ Hz.[41] The LIFDI mass spectrum showed

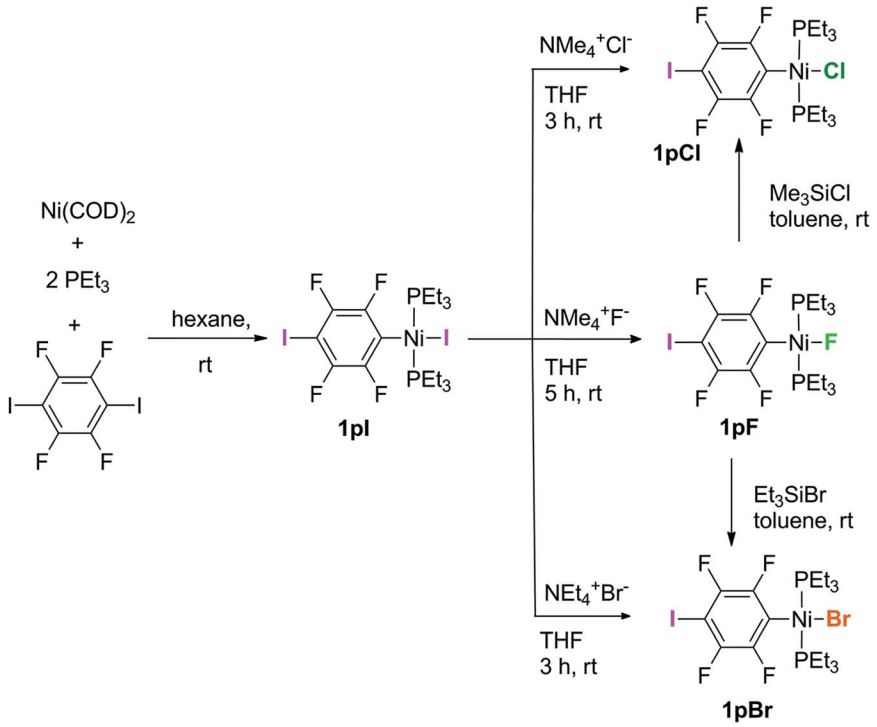

Scheme 3 Synthetic routes to complexes **1pI**, **1pF**, **1pCl** and **1pBr**.

a molecular ion [M^+] base peak (100%) at 587.99 with appropriate isotopic peaks.

The reaction of **1pI** with [NMe_4]Cl in THF at room temperature gave rise to a yellow solution of **1pCl**. Alternatively, complex **1pCl** could be synthesised rapidly and more efficiently by reacting a solution of **1pF** in toluene with chlorotrimethylsilane for 15 min at room temperature (Scheme 3). The synthesis of **1pBr** paralleled the chloride analogue and used either [NEt_4]Br in THF or bromotriethylsilane in toluene.

Synthesis of *trans*-[NiX(2,3,5,6-C_6F_4I)(PEt_2Ph)$_2$], 2pI (X = I) and 2pF (X = F)

The electronic structure of the spectator ligands on the metal centre may have a significant effect on the halogen-bonding interaction, as demonstrated by earlier work.[36] To investigate this effect on the solid-state structures, the triethylphosphine ligands on the complexes were replaced with diethylphenyl phosphine. The complex *trans*-[NiI(2,3,5,6-C_6F_4I)(PEt_2Ph)$_2$] **2pI** was prepared in a similar manner to the PEt_3 analogue. The nickel iodide **2pI** obtained was converted to the nickel fluoride **2pF** by reaction with [NMe_4]F (64% yield). NMR data for **2pI** and **2pF** corresponded closely to those of **1pI** and **1pF**. The complex **2pF** was also characterised by its LIFDI mass spectrum, which showed a molecular ion [M^+] base peak (100%) at 684.00.

Synthesis of *trans*-[NiX(2,3,4,5-C_6F_4I)(PEt_3)$_2$], 1oX, X = I, F, Cl and Br

Our next target was to change the position of the halogen-bond donor on the fluoroaromatic ring in order to compare the effect of the electron-withdrawing fluorine atoms *ortho* to the iodine and to change the relative orientation of the halogen-bond donor and acceptor groups. The synthesis of complexes from 1,2-diiodotetrafluorobenzene proceeded similarly to those from 1,4-diiodotetrafluorobenzene. The reaction of Ni(PEt_3)$_2$(COD) with 1,2-diiodotetrafluorobenzene gave rise to *trans*-[NiI(2,3,4,5-C_6F_4I)(PEt_3)$_2$] **1oI** in 67% yield. The $^{31}P\{^1H\}$-NMR spectrum of the product exhibited a singlet at δ 10.3 for the two equivalent phosphorus atoms. The ^{19}F-NMR spectrum revealed four resonances for the four aromatic fluorine atoms that were assigned with the help of ^{19}F–^{19}F COSY spectroscopy.

The product of the reaction between **1oI** and [NMe_4]F yielded *trans*-[NiF(2,3,4,5-C_6F_4I)(PEt_3)$_2$] **1oF**. The fluoride resonance was observed in the ^{19}F-NMR spectrum at δ −397.8 as a triplet of doublets as a result of phosphorus coupling (J_{FP} = 46 Hz), and a four-bond coupling to the aromatic fluorine *ortho* to the metal centre (J_{FF} = 9 Hz). Four further ^{19}F NMR resonances were observed in the aromatic region. The $^{31}P\{^1H\}$ NMR spectrum exhibited a doublet at δ 9.4 (d, J = 46 Hz). The synthesis of **1oCl** and **1oBr** followed the same pattern as for **1pCl** and **1pBr**.

A further minor product of reaction of **1oI** with [NMe_4]F exhibited resonances at δ −131.4 and at δ −150.2 in the ^{19}F-NMR spectrum and a peak at δ 27.3 in the $^{31}P\{^1H\}$-NMR spectrum. Single crystals of this species were obtained from hexane/benzene and allowed us to identify it as the η^2-tetrafluorobenzyne complex of Ni(PEt_3)$_2$, Ni(PEt_3)$_2$(η^2-C_6F_4) (see ESI‡). The spectra and structure are similar to benzyne complexes reported in the literature.[42–45]

The energetics of halogen bond formation in solution have been reported for complexes such as *trans*-[NiF(C_5NF_4)(PEt_3)$_2$] with C_6F_5I.[38] We attempted to determine the energetics of the self-complementary interactions of complex **1pF** or **1oF** by measuring ^{19}F-NMR spectra as a function of concentration. However, the solubility of both complexes **1pF** and **1oF** proved insufficient to obtain reliable data.

Crystal structures

Single crystals of complexes **1pX** were obtained by solvent diffusion. Selected intramolecular bond lengths and angles for X-ray crystal structures of **1pF**, **1pCl**, **1pBr** and **1pI** are given in Table 1; intermolecular distances and angles are given in Table 2.

For **1pF** the fluoroaromatic ring is oriented almost perpendicular to the square plane of the metal coordination centre, 85.2(2)°. The crystal structure comprises chains of the nickel complexes linked by short C–I···F(Ni) halogen bonds (I···F 2.655(5) Å, C–I···F 180.0°, I···F–Ni 180.0°, Fig. 1a). The parallel sets of linear chains align with the *b*-axis and form layers in the ab plane. Complexes **1pCl**, **1pBr** and **1pI** (Fig. 1b–d, Table 1) crystallize as antiparallel zig-zag chains with molecules linked by a C–I···X–Ni halogen bonds. The Ni···Ni···Ni angle (Table 2) may be taken as an estimate of the zig-zag angle and indicates a slight zig-zag for X = Cl, Br and I (Ni···Ni···Ni 159.91(1),

Table 1 Selected intramolecular bond lengths (Å), bond angles (°) and torsion angles (°) of **1pX** (X = F, Cl, Br, I), **2pI** and **1oX** (X = F, Cl, I) determined at 110 K

Complex	I1–$C_{aromatic}$	Ni–P1	Ni–X	Ni–C1
1pF	2.096(11)	2.208(2)	1.837(5)	1.873(13)
1pCl	2.082(2)	2.2086(5)	2.2035(5)	1.881(2)
1pBr	2.082(2)	2.2176(6)	2.3385(3)	1.881(2)
1pI	2.092(6)[a]	2.224(2)	2.5221(9)	1.877(6)
2pI	2.089(2)[a]	2.2200(6)	2.5348(4)	1.902(2)
1oF	2.111(6)	2.218(2)	1.841(4)	1.890(6)
1oCl[b]	2.095(4)	2.270(5)	2.201(5)	1.899(5)
1oI(α)	2.096(4)[c]	2.225(1)	2.5332(6)	1.907(4)
1oI(β)	2.098(3)[c]	2.234(1)	2.5358(4)	1.893(3)
1oI(γ)	2.088(5)[c]	2.231(1)	2.5337(8)	1.908(5)

Complex	X–Ni–C1	P1–Ni–P2	P1–Ni–X	P1–Ni–C1–C2	Angle between metal plane and ring plane[d]
1pF	180.0	177.1(1)[e]	91.46(6)	85.2(3)	85.2(2)
1pCl	175.82(5)	175.65(2)	89.12(2)	87.9(1)	82.13(4)
1pBr	176.61(6)	176.94(2)	88.85(2)	86.2(2)	85.60(5)
1pI	178.3(2)	178.33(7)	89.55(5)	84.0(5)	85.14(16)
2pI	175.36(2)	175.36(2)	89.59(2)	88.7(2)	89.07(5)
1oF	179.3(3)	173.12(9)	88.60(16)	85.3(6)	84.4(2)
1oCl[b]	178.1(3)	171.0(4)	89.67(16)	90.1(4)	85.1(1)
1oI(α)	173.8(1)	177.33(5)	88.87(3)	89.17(3)	90.0
1oI(β)[b]	179.8(1)	174.72(3)	89.67(2)	89.6(3)	89.3(1)
1oI(γ)	178.1(1)	169.72(6)	92.67(4)	84.0(4)	86.8(1)

[a] Bond I2–C4. [b] Measurements are for the major component. [c] Bond I2–C2. [d] Metal plane Ni–P1–P2–C1–X. [e] Angle (P1–Ni–P1′).

Table 2 Intermolecular distances and the angles of **1pX**, (X = F, Cl, Br, I), **2pI**, **1oF**, **1oCl**, and **1oI** determined at 110 K

Compound	Intermolecular I···X/Å	R^{A}_{IX} [a]	R^{B}_{IX} [a]	C–I···X/°	I···X–Ni/°	Angle/° between adjacent metal planes [b]	Angle/° between adjacent ring planes	Ni···Ni···Ni/°
1pF	2.655(5)	0.76	0.77	180.0	180.00	0.0	0.0	180.00
1pCl	3.2414(5)	0.84	0.87	167.09(5)	146.83(2)	72.69(2)	88.01(8)	159.91(1)
1pBr	3.3320(3)	0.85	0.87	167.55(6)	143.31(1)	70.91(3)	87.8(1)	158.95(1)
1pI	3.4970(6)	0.86	0.88	168.0(2)	139.18(3)	67.41(8)	87.4(3)	156.79(2)
2pI	3.6791(4)	0.90	0.93	167.39(6)	158.22(1)	0.0	0.0	180.00
1oF	2.941(5)	0.84	0.85	173.2(2)	172.4(2)	72.3(3)	31.7(3)	113.55(2)
1oCl major	3.342(6)	0.87	0.90	169.4(2)	158.1(3)	54.5(2)	26.1(2)	112.1(1)
1oCl minor	3.26(2)	0.84	0.87	178.7(4)	171.8(8)	72.1(7)	26.1(2)	108.8(2)
1oI(α)	3.5961(4)	0.88	0.91	178.5(1)	144.16(2))	77.1(1)	0.0	97.00(1)
1oI(β)	3.7456(4)	0.92	0.95	151.7(1)	133.48(1)	45.1(1)	12.4(2)	124.80(1)
1oI(γ)	4.0752(7)	1.00	1.03	169.2(1)	161.63(2)	64.6(1)	39.5(2)	101.06(1)

[a] The normalised distance, R, is defined according to Lommerse *et al.*[48] $R^{A}_{IX} = d(I\cdots X)/(r^{A}_{I} + r^{A}_{X})$, where r^{A}_{I} and r^{A}_{X} are the Alvarez van der Waals radii[46] of the iodine atom, and halogen (F 1.46, Cl 1.82, Br 1.86 or I 2.04 Å), respectively, in the C–I···X–Ni halogen bond. $R^{B}_{IX} = d(I\cdots X)/(r^{B}_{I} + r^{B}_{X})$, where r^{B}_{I} and r^{B}_{X} are the Bondi van der Waals radii[47] of the iodine atom, and halogen (F 1.47, Cl 1.75, Br 1.83 or I 1.98 Å), respectively, in the C–I···X–Ni halogen bond. [b] Metal plane Ni–P1–P2–C1–X.

158.95(1), 156.79(2)°, respectively, *cf.* 180° for X = F). The intermolecular distances I···X are substantially less than the sum of van der Waals radii (R^{A}_{IX} 0.84–0.86; R^{B}_{IX} 0.84–0.87; see Table 2 for definitions of distances, R^{A}_{IX} and R^{B}_{IX}, which represent the fraction of the sum of van der Waals radii[46,47] of the two interacting atoms I and X), but show smaller reductions than observed for **1pF** (R^{A}_{IF} 0.76; R^{B}_{IF} 0.77). The C–I···X angles deviate slightly from linear (*ca.* 167°) while the I···X–Ni angles lie in the range 139–147°. The torsional angles between adjacent metal coordination planes in the chains are *ca.* 70°, while adjacent benzene ring planes are approximately orthogonal (*ca.* 88°, Table 2). In addition, the crystal structure of the minor dinuclear product, [*trans*-NiBr(PEt_3)$_2$]$_2$(μ-2,3,5,6-C_6F_4) was determined (see ESI‡ and Scheme 4).

Single crystals of **2pI** suitable for X-ray crystallography were grown as dark yellow blocks by solvent diffusion (Fig. 2). The three aromatic rings present in the structure orient themselves away from each other and there are neither inter- nor intramolecular π–π interactions. Unlike **1pI**, the Ni coordination planes and the tetrafluoroiodophenyl rings are parallel to one another. The complexes pack with zig-zag halogen-bonded chains, which run parallel (and anti-parallel) to the *b*-axis. The C–I···I–Ni halogen bonds (I···I 3.6791(4) Å, C–I···I 167.39(6)°, I···I–Ni 158.22(1)°) are markedly longer than those of **1pI** (Table 2). Attempts to obtain single crystals of **2pF** suitable for X-ray crystallography were fruitless.

Single crystals of **1oF**, **1oCl** and **1oI** were obtained that were suitable for X-ray crystallography.‖ Selected intramolecular distances and angles are given in Table 1 and intermolecular distances and angle in Table 2. The crystal structures are illustrated in Fig. 3. It might be expected that the Ni–C distances in the **1pX** series would be shorter than those in the **1oX** series because of the *ortho*-fluorine effect.[49] Although the Ni–C distances are consistently shorter for **1pX** than for their **1oX** analogues, the differences are of marginal significance. The differences in the C–I distances are insignificant. In all of the **1oX** halogen-bonded complexes, the iodine on the ring in the *ortho* position causes a pronounced zig-zag of the complexes, as described by the Ni···Ni···Ni angle (96 ≤ Ni···Ni···Ni ≤ 125°, Table 2). The normalised distances of the I···X contacts R^{B}_{IX} are 0.85 for **1oF**, 0.90 for **1oCl** (major) and 0.91–1.03 for **1oI**, much larger than for **1pX** analogues.

Single crystals of **1oI** were obtained as three polymorphs, **1oI(α)** crystalized from hexane, and the other two (**1oI(β)** and **1oI(γ)**) from $CHCl_3$ layered with hexane. Polymorph **1oI(α)** shows the typical C–I···I–Ni halogen-bonding contacts (3.6100(3) Å). The polymorphs from chloroform exhibited the same patterns of halogen bonding but with progressively longer contacts. The C–I···I–Ni contact is 3.7456(4) Å for **1oI(β)**, (major component), while **1oI(γ)** has two independent molecules in the unit cell, one of which has a C–I···I–Ni distance of 4.0752(7) Å and the other shows no halogen bonding at all. The changes in halogen-bonding geometry accompany changes in orientation of molecules along the halogen-bonded chains, exemplified by the twisting of the ring planes of adjacent molecules with respect to one another for **1oI(β)** and **1oI(γ)**, but coplanar arrangement in **1oI(α)**.

Variable-temperature X-ray crystallographic studies of 1pF′ and 1pF

The effects of temperature and pressure on C–Cl···X–M halogen bonds (X = Cl, Br) have been studied by Mínguez Espallargas *et al.*, illustrating the compressibility of these non-covalent interactions.[16,50] In order to quantify the temperature dependence of our system, crystals of **1pF** were selected as they showed the strongest X-bonding interaction of the series of complexes prepared. A crystal of **1pF** was cooled to 111 K and the structure determined, warmed to 200 K and analysed again, and finally warmed to 240 K and the structure obtained a third time. At 111 K and 200 K, the space group was *I*2 whereas at 240 K the space group was *Cc*. The space group change was accompanied by a change in the unit cell, suggesting a phase change between 200 and 240 K. Overlaying the structures at 200 and 240 K revealed that the major difference in structures is the position of one of the triethylphosphine ligands (Fig. S41‡). At

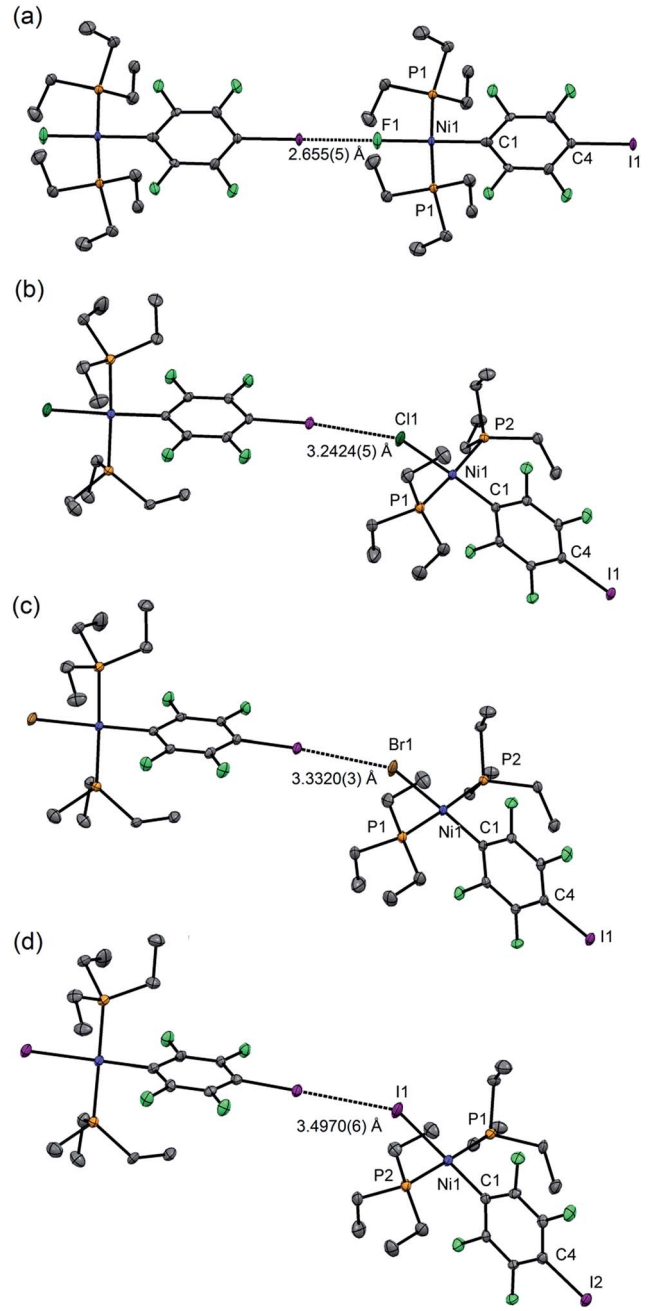

Fig. 1 Molecular structures of **1pX** (a) X = F, (b) X = Cl, (c) X = Br, (d) X = I, showing intermolecular halogen bonds. Displacement ellipsoids at 50% probability level. Hydrogen atoms not shown. Three-molecule chains are illustrated in the ESI.†

the higher temperature, the triethylphosphines are no longer related by a two-fold rotation and one is disordered in two positions (see ESI‡). The variable temperature X-ray crystallographic data of **1pF** show that a 4.5% reduction in the volume per molecule (*V*/*Z*) is observed when the temperature is changed from 240 K to 200 K and *ca.* 2% reduction in the volume is observed from 200 K to 111 K (Table 3). The change in space group from *I*2 to *Cc* removes the linearity of the halogen-bonded chain. Nevertheless, the key angles remain close to 180°: the C–I···F angle is 177.8(8), I···F–Ni 164.8(7) and the Ni···Ni···Ni angle is

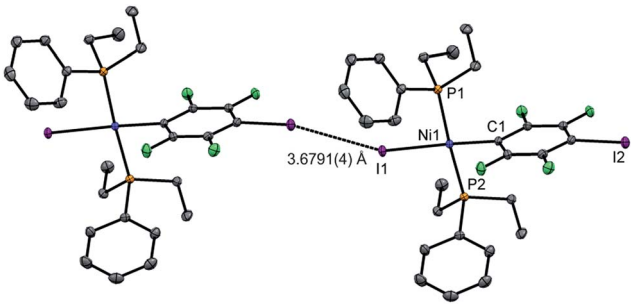

Fig. 2 Molecular structure of **2pI** showing intermolecular C–I···I–Ni halogen bond. Displacement ellipsoids at 50% probability level. Hydrogen atoms not shown. A three-molecule chain is illustrated in the ESI.‡

171.5(3)°. Although changes in bond lengths to nickel were insignificant, the intermolecular distance between the fluoride on the metal centre and the iodine on the fluoroaromatic ring decreased with temperature by 0.055(7) Å from 240 to 111 K. The normalised halogen-bonded distance R^{B}_{IF} remains below 0.80 throughout the temperature range (Table 2).

Solid-state NMR spectroscopic studies

Magic-angle spinning solid-state NMR (MAS SSNMR) spectroscopy offers an opportunity to learn more about the halogen-bonding interactions.[51–53] We have found one other example of a ^{19}F-MAS SSNMR spectrum for a nickel fluoride complex[54] and one example of calculated ^{19}F tensors for some cobalt fluorides.[55] The fluoride bound to the nickel centre can act as a ^{19}F-MAS SSNMR spectroscopic handle because the chemical shift is very sensitive to the fluoride environment[36] and appears at high field with no overlap from other resonances. ^{19}F-MAS SSNMR spectroscopy was used to analyse the effect on the fluoride resonance of halogen-bonding interactions in complexes **1pF** and **1oF**. The complex *trans*-[NiF(C$_6$F$_5$)(PEt$_3$)$_2$] **3F**, which has no halogen-bond donor atom on its backbone was also analysed by ^{19}F-MAS SSNMR spectroscopy for comparison.[41] The spectrum of **1pF** (Fig. 4) shows the isotropic chemical shift of the nickel fluoride at δ −359.8 with numerous spinning side bands (black dots in Fig. 4). The other peaks in the range of δ −100 to −160 arise from the resonances of the fluoroaromatic ring. Measurement at various spinning speeds allowed simulation of spectrum and determination of the components of the chemical shift anisotropy (CSA) tensor and identification of δ_{iso} of the fluoride resonance. Expansions of the isotropic region of the spectra are shown in Fig. 5 and the trends in the CSA components in Fig. 6.

The components of the anisotropic chemical shift tensor are labelled as δ_{11}, δ_{22} and δ_{33}, where δ_{11}, is the least shielded component and δ_{33} is the most shielded component ($\delta_{11} \geq \delta_{22} \geq \delta_{33}$).[56] For **1pF**, the simulations show δ_{11} at δ −165, δ_{22} at δ −266 and δ_{33} at δ −645. The ^{31}P{^{1}H} spectrum of **1pF** (see ESI‡) reveals a coupling $^{2}J_{PF} = 42 \pm 3$ Hz, similar to the value observed in solution (46 Hz). We were unable to obtain the J_{PF} coupling in the ^{19}F-MAS SSNMR spectra for **1oF** and **3F**.

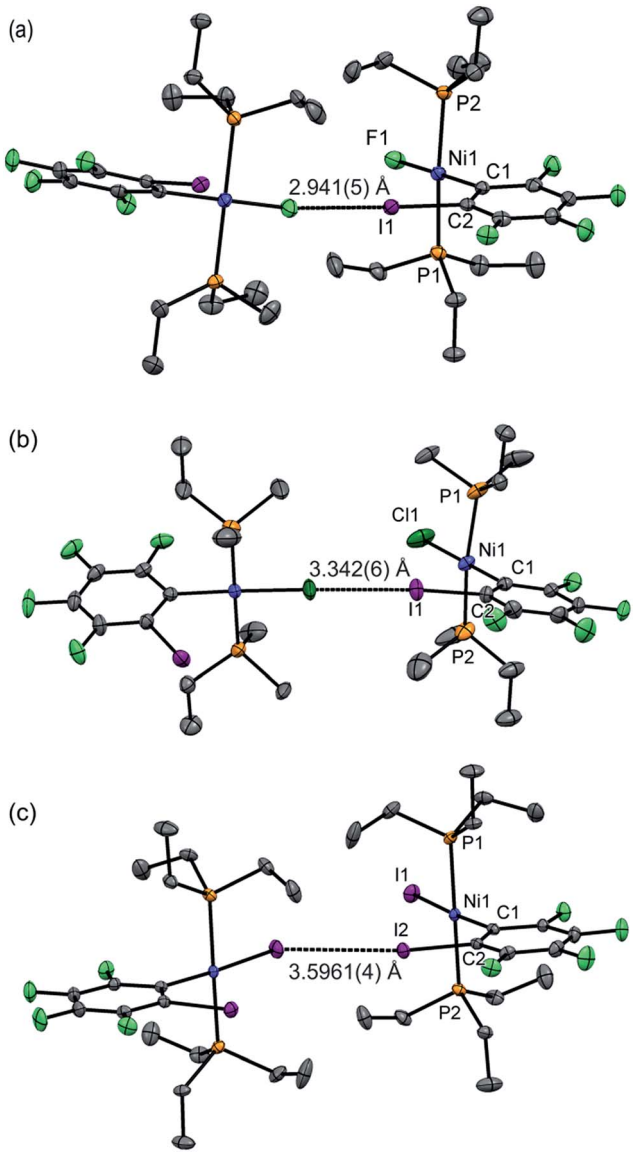

Fig. 3 Molecular structures of **1oX** (a) X = F, (b) X = Cl, (c) X = I, showing intermolecular C–I···X–Ni halogen bonds. The structure of **1oCl** is disordered (see Table 2). Only the major component is shown. Hydrogen atoms and some methyl groups omitted for clarity. Displacement ellipsoids at 50% probability level. Three-molecule chains are illustrated in the ESI.‡

In addition, the structure of the gas-phase model *trans*-[NiF(2,3,5,6-C_6F_4I)(PMe_3)$_2$] and its halogen-bonded complex with C_6F_5I were determined by DFT methods showing a (C)I···F(Ni) distance of 2.749 Å. DFT simulation of the ^{19}F-MAS SSNMR spectra of both these species showed that δ_{11} lies along the Ni–F bond, δ_{22} lies parallel to the Ni–P bonds and δ_{33} lies perpendicular to the coordination plane of nickel (Fig. 6, lower pane). Moreover, the CSA calculated by DFT methods for *trans*-[NiF(2,3,5,6-C_6F_4I)(PMe_3)$_2$] and *trans*-[NiF(2,3,5,6-C_6F_4I)(PMe_3)$_2$]···IC_6F_5 show that the changes in the shielding of the δ_{11} and δ_{22} components are small and of opposite sign, thus minimizing their effect on the isotropic shift.

Table 3 Selected variable-temperature X-ray crystallographic data for complex **1pF**

	Space group/temperature, K		
	*I*2/111[a]	*I*2/200	*Cc*/240
V/*Z*/Å^3	577.09(5)	588.17(4)	614.7(1)
(C)I···F(Ni)/Å	2.652(3)	2.683(5)	2.707(7)
Ni–F/Å	1.839(4)	1.832(5)	1.855(10)
Ni–C/Å	1.872(10)	1.879(10)	1.88(2)
Ni–P/Å	2.211(1)	2.214(1)	2.209(5)
C–I···X/°	180.0	180.0	177.8(7)
I···X–Ni/°	180.0	180.0	164.8(7)
Angle/° between adjacent metal planes[b]	0.0	0.0	26.3(7)
Angle/° between adjacent ring planes	0.0	0.0	4.9(10)
Ni···Ni···Ni/°	180.0	180.0	171.50(3)

[a] Independent determination from 110 K study reported in Tables 1 and 2. [b] Metal plane Ni–P1–P2–C1–X.

The isotropic chemical shift δ_{iso} of the fluoride resonance of **3F** was observed at δ −393.9 in the ^{19}F-MAS SSNMR spectrum (Table 4, Fig. 5), in good agreement with the solution-state fluoride resonance at δ −394.3 (in C_6D_6) for the same complex. In contrast, the solution-state fluoride resonance of **1pF** appeared ∼29 ppm to higher field at δ −388.3 than its solid state isotropic chemical shift (δ −359.8). Similarly, the solution-state fluoride resonance of **1oF** was observed ∼25 ppm to higher field at δ −397.9 than its solid state counterpart. Thus the solid-state NMR spectra provide strong evidence of deshielding of δ_{iso} with increasing halogen-bond interaction. Table 4 gives values of the SSNMR parameters. The δ_{33} component is systematically deshielded upon increasing halogen bond strength, mirroring what is observed in the isotropic chemical shift, and there is also a reduction in the span, Ω. Since the DFT calculations indicate a minimal contribution of δ_{11} and δ_{22} to the changes in δ_{iso}, we conclude that the changes in δ_{33} are dominated by the effect of halogen bonding. The deshielding of the NiF resonance is also consistent with the effect of addition of C_6F_5I to *trans*-[NiF(C_5NF_4)(PEt_3)$_2$] in solution.[36,38] A very large chemical shift anisotropy was also reported for another nickel fluoride complex,[54] and very strong paramagnetic shielding was observed perpendicular to the metal phosphorus bond for terminal phosphido complexes in their ^{31}P-MAS SSNMR spectra.[57] Large chemical shift anisotropies have recently been measured and calculated for metal hydrides.[58,59]

The paramagnetic contribution to the components of the chemical shift tensor are understood *via* second order perturbation theory as being affected by the angular momentum operator $\hat{L}_i$ ($i = x, y, z$) which couples occupied orbitals to vacant orbitals after a 90° rotation about the direction i.[60,61] In this case δ_{33} lies in the out-of-plane direction z and is rotated by $\hat{L}_y$ into the x direction that coincides with the vacant M–F σ* orbital. It is this orbital that is affected by the halogen bonding both through electrostatic effects and through interaction with the C–I σ and σ* orbitals.[52] As the δ_{33} component is deshielded

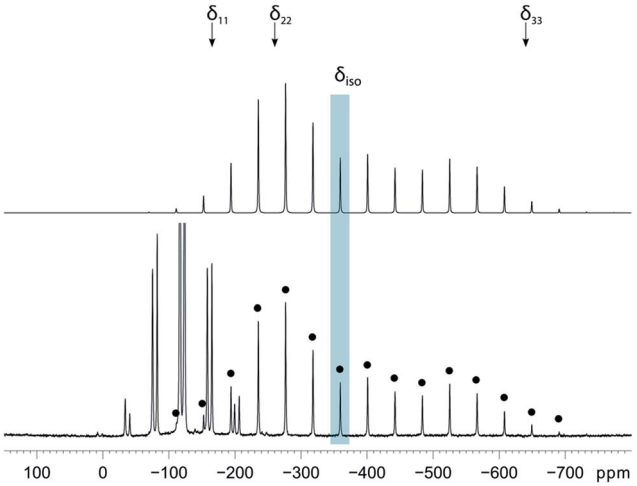

Fig. 4 ^{19}F-MAS SSNMR spectrum of **1pF**. Top: best fit simulated spectrum for the Ni–F resonance with the positions of the shielding tensor marked. Bottom: experimental spectrum. Spinning speed 15.6 kHz. Signals arising from the fluorinated benzene ligand (−110 to −160 ppm) are truncated. The black dots indicate the NiF peak and its spinning side bands. The blue bar indicates δ_{iso}.

upon formation of the halogen bond, the energy gap between these two orbitals must decrease.

Discussion of trends in halogen bonding

This study establishes that nickel halide complexes *trans*-[NiX(C_6F_4I)(PR_3)$_2$] form intermolecular C–I···X–M halogen bonds by self-recognition in the solid state, leading to halogen-bonded chain motifs. Their crystal structures provide extensive geometric data for these halogen bonds that demonstrate a marked difference between the fluoride complexes and those of the other halides. The strengths of halogen bonds may be compared by the normalised distances (here R^{A}_{IX} or R^{B}_{IX}, see Table 2).[16,48] As for other strong halogen bonds, C–X···X′–M halogen bonds adopt a characteristic angle C–X···X′ close to 180°; the X···X′–M angle, however, is typically in the 110–140° range for X′ = Cl, Br, I,[30,31,62] but can vary more widely[23,63] as the halide ligand exhibits a negative electrostatic potential attractive to halogen bond donors and other Lewis acidic moieties at all angles of approach.[64] Despite their established greater strength,[36–39] there have been no systematic crystallographic studies prior to this study that establish C–X···F–M halogen bond geometries and, in particular typical X···F–M angles.

In this study we examined the class of C–I···X–M halogen bonds through a series of systematic changes and perturbations, by monitoring the geometry as a function of: (i) halide ligand, X, (ii) regiochemistry of halogen-bond donor, I (**1pX** *vs.* **1oX**) (iii) influence of ligand sphere of the metal on halogen-bond acceptor, X, by changing PEt_3 for $PPhEt_2$, (iv) the influence of crystalline environment, by comparison of three polymorphs tnqh_x2026;of **1oI**, and (v) the effect of temperature, in a study of **1pF**.

Common features of halogen-bonded chain structures

1pF forms linear chains, whereas the structures of **1pX** (X = Cl, Br, I) and **1oX** (all X) form zig-zag chains. The zig-zag angles of the chains of **1pCl**, **1pBr** and **1pI** are characterised by

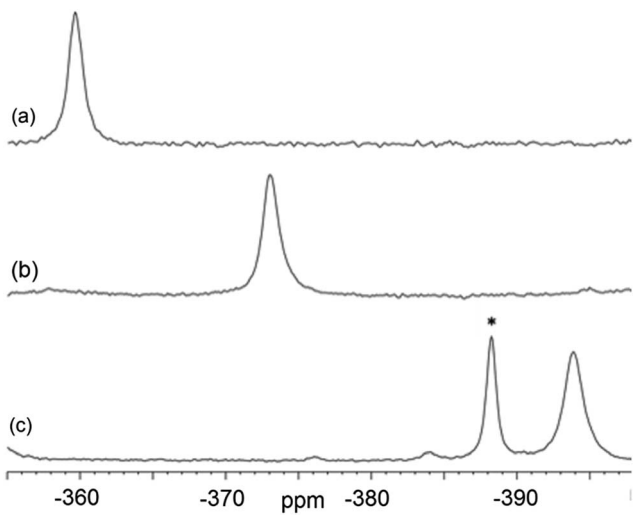

Fig. 5 Expansion of isotropic region of ^{19}F-MAS SSNMR spectrum of (a) **1pF**, (b) **1oF** and (c) *trans*-[NiF(C_6F_5)(PEt_3)$_2$] **3F** with no halogen bond, (asterisk solvated complex impurity <4%).

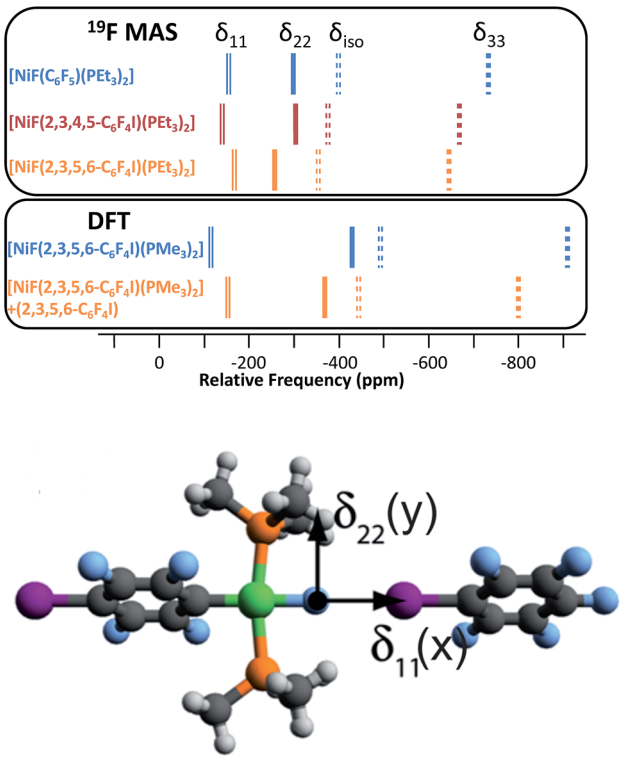

Fig. 6 Top: positions of the observed (^{19}F-MAS SSNMR) principal tensor components (δ_{11}, δ_{22}, δ_{33}) and isotropic shift (δ_{iso}) for **3F**, **1oF** and **1pF**. Middle: values of δ_{11}, δ_{22}, δ_{33}, and δ_{iso} determined by DFT calculations for *trans*-[NiF(2,3,5,6-C_6F_4I)(PMe_3)$_2$] and its halogen-bonded complex with C_6F_5I. Bottom: calculated structure of C_6F_5I···FNi(2,3,5,6-C_6F_4I)(PMe_3)$_2$ showing orientation of CSA tensor (δ_{33} component is perpendicular to the plane of the page).

Table 4 Chemical shifts in solution in C_6D_6 (40 μM) and ^{19}F-MAS SSNMR parameters for **1pF**, **1oF** and **3F**[a]

Sample	Solution δ	δ_{iso}	Ω	κ	δ_{11}	δ_{22}	δ_{33}
1pF	−388.3	−359.8(2)	480(10)	0.58(3)	−165	−266	−645
1oF	−397.9	−373.0(2)	530(10)	0.40(3)	−143	−302	−673
3F	−394.3	−393.9(2)	575(10)	0.50(3)	−154	−298	−729

[a] Chemical shift tensor parameters,[56] δ_{iso} Isotropic chemical shift, $\delta_{iso} = (\delta_{11} + \delta_{22} + \delta_{33})/3$, Ω Span of the CSA powder pattern, $\Omega = \delta_{11} - \delta_{33}$, κ Skew, measures the asymmetry of the powder pattern, $\kappa = (\delta_{22} - \delta_{iso})/\Omega$.

Ni···Ni···Ni angles in the 155–160° range (see figures in ESI‡). The angles between adjacent metal coordination planes and the angles between adjacent benzene ring planes also show marked differences between **1pF** on the one hand and **1pCl**, **1pBr** and **1pI** on the other (Table 2). The zig-zag in the *ortho* series is dominated by the 60° angle imposed by the *ortho* substitution, which causes a major reduction in the Ni···Ni···Ni angle compared to the *para* analogues (**1pF** 180° and **1oF** *ca.* 114°, **1pCl** *ca.* 160° and **1oCl** *ca.* 112°, **1pI** *ca.* 157° and **1oI(α)** *ca.* 97°). Both the angle between adjacent ring planes and the Ni···Ni···Ni angle are significantly smaller for **1oI(α)** than for the fluorine and chlorine analogues.

Trend with halide ligand for 1pX and 1oX: distance

The normalised distances (Table 2) range from 0.76 for **1pF** to 0.90 for **2pI** (Alvarez radii, R^{A}_{IX}) or 0.77 to 0.93 (Bondi radii, R^{B}_{IX}).[46,47] The normalised distance is markedly smaller for **1pF** than for **1pCl**, **1pBr** and **1pI**. Nevertheless, there is a small increase from Cl to Br and from Br to I. Thus the large negative electrostatic potential of fluorine is the dominant effect[38,64] and the changes between the other halogens are smaller in this series. The trend is consistent with the observations for hydrogen-bond acceptor behaviour of halide ligands, *e.g.* D–H···X–M, where the H-bond donor D = N, O (or even C). Normalised hydrogen bond distances follow the trend $R^{B}_{HF} \ll R^{B}_{HCl} \leq R^{B}_{HBr} < R^{B}_{HI}$.[64] Overall, the geometric results are consistent with fluoride ligands being much stronger halogen-bond and hydrogen-bond acceptors than their heavier congeners. Our results on **1pCl** and **1pBr** are also comparable to those recorded for the co-crystals of 1,4-($C_6F_4I_2$) with PdX(PCP) (X = Cl, Br), but the Pd–F complexes were not synthesised.[31]

The normalised distances for the **1pX** series are considerably smaller than for the **1oX** series, especially for X = F (Table 2). Considering that the regiochemistry has a very minor effect on the Ni–C and the C–I distances, there is no evidence that the changes in the halogen-bond distance have an electronic origin. On the other hand, they can be rationalised on steric grounds since the σ-hole of the **1pX** halogen-bond donor atom is more accessible than that in the **1oX** series. The trend in normalised distances with halide ligand for the **1oX** series, however, resembles that for **1pX**.

Trend with halide ligand for 1pX and 1oX: angle

Halogen bonding interactions are directional forces because of the anisotropic charge distribution around halogen atoms. The charge distribution is compressed along the C–I axis, creating the positive potential *trans* to the C–I bond, leading to C–I···X angles that are close to linear.[16,18,48] Halide ligands (M–X) exhibit a similar anisotropy, albeit with a negative potential in all directions at separations appropriate for intermolecular interactions. Brammer *et al.*[30,64] reported the calculated electrostatic potential around the halogen in palladium halide complexes, *trans*-[PdX(CH_3)(PH_3)$_2$]. They showed that the most negative value in the molecular plane is consistent with I···X–M angles at 155° with a range of 130–180° range when X = F, whereas the other halogens exhibited minima at *ca.* 124° and a range of *ca.* 110–140°.[64] In the **1pX** series of complexes, C–I···X angles are close to linear, consistent with typical halogen-bond behaviour (**1pF** 180°; **1pCl**,

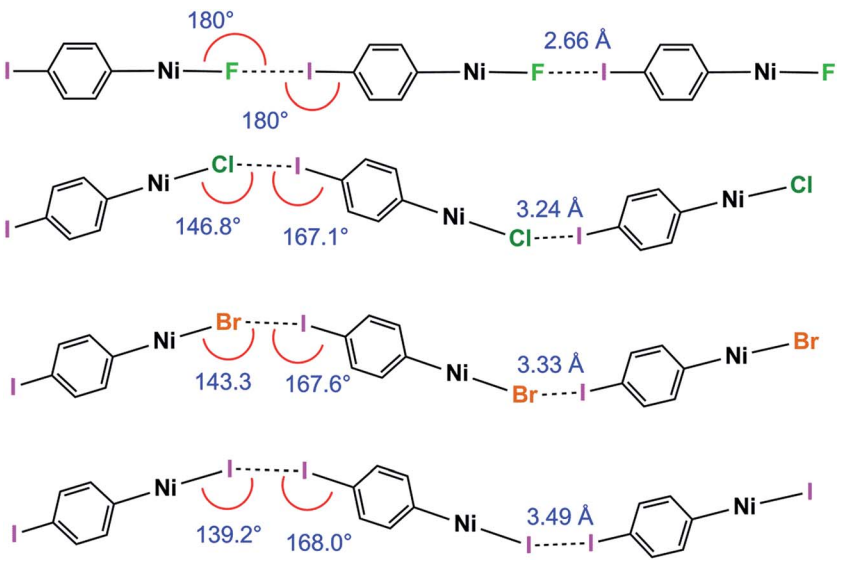

Scheme 5 Halogen bond length and C–I···Ni and I···X–Ni angles for the **1pX** series (phosphines and aromatic fluorines omitted, for esd's see Table 2).

1pBr, **1pI** all close to 167°, Scheme 5). The I···X–Ni angle of **1pF** is 180°, exceeding the I···X–Ni angles for the other halides, which are in the range 139–147° (Table 2, Scheme 5). This result is in keeping with the analysis of angular variation of the halide negative electrostatic potential mentioned above, and is consistent with more restricted steric access to the halide ligand at lower I···X–Ni angles, since Ni–F and I···F separations are markedly shorter than for other Ni–X and I···X.

The C–I···X angles are again similar and close to linear across the **1oX** series. The variation in the I···X–Ni angle is more marked, moving from 172.4(2)° to 158.1(3)° and 143.66(1)° along the series **1oF**, **1oCl**, **1oI(α)** (Scheme 6, Table 2), which is qualitatively consistent with the trend in location of electrostatic potential minima at the halide ligand.

Effect of phosphine substituents

The change in phosphine from **1pI** with PEt_3 to **2pI** with PEt_2Ph causes a marked increase in the halogen-bond distance, indicating the sensitivity of the halogen bond to the ligand sphere of the metal. There are no solution-phase measurements on PEt_2Ph complexes for comparison although an increase in enthalpy of C–I···F–Ni halogen bonding when replacing PEt_3 ligands by PCy_3 has been reported.[38]

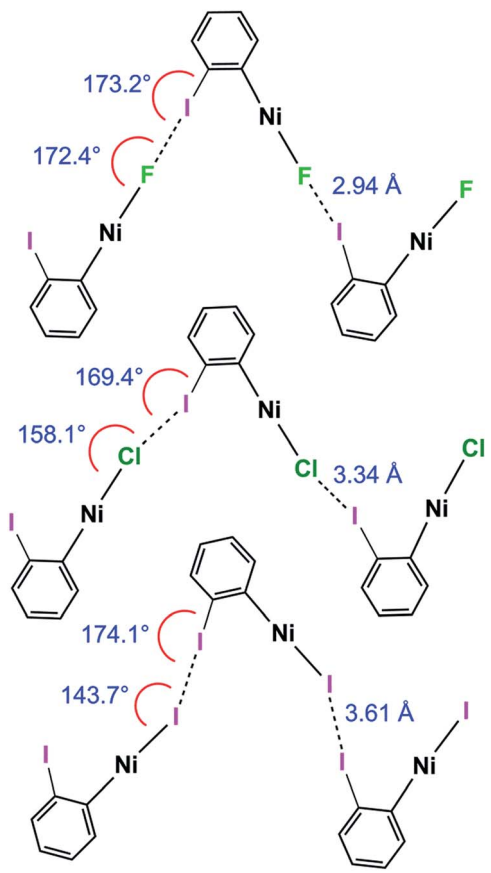

Scheme 6 Halogen bond length and C–I···Ni and I···X–Ni angles for **1oF**, **1oCl** and **1oI(α)** (phosphines and aromatic fluorines omitted, for esd's see Table 2).

Trend with polymorph for 1oI

The crystallisation of three solvent-free polymorphs of **1oI** allowed the effect of crystalline environment on formation and geometry of the C–I···I–Ni halogen bond to be examined. The three polymorphs provide four different crystalline environments as there are two crystallographically independent molecules in **1oI(γ)**. The I···I distances vary from 3.5961(4) Å in **1oI(α)** to 3.7456(4) in **1oI(β)** to 4.0752(7) Å **1oI(γ)**, whereas the second independent molecule exhibits no halogen-bonding interaction. The different crystalline environments also lead to changes in halogen-bond angles C–I···I and I···I–Ni, and to changes in relative orientation of neighbouring molecules in the halogen-bonded chains (Table 2).

Trend with temperature for 1pF

The study of the structure of **1pF** using one single crystal at three temperatures** enabled the perturbing effect of temperature on the geometry of the C–I···F–Ni halogen bond to be examined. The halogen-bonded distance remains well over 20% shorter than the sum of the van der Waals radii (R^{A}_{IF}, R^{B}_{IF} < 0.8), and C–I···F and I···F–Ni angles remain close to linearity, across the temperature range studied (111–240 K). Two previous studies of halogen-bonding as a function of temperature also reveal only very small changes in halogen bond angles. Forni *et al.* reported changes in halogen-bond distance of 0.052(2) Å (C–I···N), 0.030(2) Å (C–I···O) and 0.059(2) Å (C–Br···N) over the temperature range 90–292 K.[65] Brammer *et al.* reported changes of 0.070(2) Å (C–Cl···Cl(M)) and 0.079(1) Å (C–Cl···Br(M)) over the temperature range 30–300 K.[16,50] These values are consistent with the changes observed here, *viz.* 0.055(7) Å. Such changes are greater than observed for intramolecular distances, but smaller than those for other intermolecular separations, which reflects the strength of these halogen bonds and, in conjunction with their directionality, underlines their utility in supramolecular assembly.

Conclusions

Our design strategy for a full range of structures of the type *trans*-[NiX(C_6F_4I)(PR_3)$_2$], for all halogens X, reveals supramolecular chain structures containing self-complementary halogen-bonding motifs linked by C–I···X–Ni halogen bonds. This methodology fulfils the objectives for thorough geometric comparisons and provides a platform for development of supramolecular assemblies with metal–fluoride complexes, which form the strongest halogen bonds. Moreover, the methods offer an entry into solid-state NMR studies of halogen bonding by use of the ^{19}F nucleus of the fluoride ligand as a spectroscopic probe that is not complicated by nuclear quadrupole effects. Such NMR studies will also enable improved comparison between halogen bonds in the solid state and solution phase. This type of comparison is rarely accessible, but is important because the solid state provides the most accurate geometric information through crystallography, while the solution phase provides the most direct experimental

means of determining interaction energies through spectroscopic titrations.

The strongest halogen bonds are formed by *trans*-[NiF(*p*-C_6F_4I)$(PEt_3)_2$], judged both by the reduction in I···X distance compared to the sum of the van der Waals distances and by the ^{19}F SSNMR chemical shift. This system contains a linear chain. Other complexes of the type *trans*-[NiX(*p*-C_6F_4I)$(PEt_3)_2$] (**1pX**, X = Cl, Br, I) exhibit zig-zag chain structures with angles C–X···I and I···X–Ni, and angles between Ni coordination planes and between ring planes that are similar for X = Cl, Br and I. The corresponding complexes *trans*-[NiX(*o*-C_6F_4I)$(PEt_3)_2$] (**1oX**, X = F, Cl, Br, I) all form chains in the solid state with more pronounced zig-zags and weaker halogen bonds than their *p*-C_6F_4I counterparts (**1pX**). The relative strengths of the halogen bonds, as judged by smaller normalised C–I···X halogen-bond distances (R^A_{IX}, R^B_{IX}), follow the pattern **1pX** > **1oX** and F > Cl ∼ Br > I, consistent with observations of hydrogen bond acceptor capabilities of halide ligands, X. The variation in the I···X–Ni angles is consistent with the location of the electrostatic potential minima associated with anisotropic charge distribution of the halide ligand, X, which have a directing effect on the halogen bond.

We have shown by comparison of three polymorphic forms of **1oI** that the crystalline environment can have a marked effect on halogen bond geometry and indeed on whether a (weaker) halogen bond is formed at all. These results emphasise the importance of examining trends in intermolecular interaction geometries in the solid state and avoiding overinterpretation of the link, for example, between intermolecular distances and interaction strength based on individual solid-state observations. The study of the crystal structure of **1pF** over the temperature range 111–240 K reveals only a small change in halogen bond length, consistent with the C–I···F–Ni halogen bond being a strong intermolecular interaction.

Finally, we have shown that it is possible to demonstrate the existence of halogen bonding in the fluoride complexes with ^{19}F-MAS SSNMR spectroscopy. With a suitable reference, *trans*-[NiF$(C_6F_5)(PEt_3)_2$] **3F**, the presence of the halogen bonds is manifest through downfield shifts in the resonance of the Ni–F as has previously been reported in solution. The ^{19}F SSNMR isotropic chemical shifts follow the order **3F** < **1oF** < **1pF** in agreement with the crystal structures, where **1pF** shows the strongest halogen-bonding interactions (smallest R_{IX} values). Comparisons between solution and solid-state NMR indicate that C–I···F–Ni halogen bonding causes deshielding of δ_{iso} by 25–30 ppm; examination of the chemical shift tensor indicates that by far the biggest contributor to the deshielding is δ_{33}, the component perpendicular to the metal coordination plane. This shift is consistent with coupling of the occupied F($2p_z$) orbital with the vacant M–F σ* orbital; it is this orbital that is influenced by the halogen bonding.

Experimental

All experiments involving oxygen- and water-sensitive materials were performed under an argon or nitrogen atmosphere, in an argon-filled glove box or standard Schlenk (10^{-2} mbar) techniques or high vacuum lines (10^{-4} mbar). Solvents (AR grade) for general use were dried over sodium, distilled and stored under argon. Solvents such as hexane and THF were collected from the Innovative Technology solvent purification system and were further dried and distilled. Deuterated solvents were dried over potassium and distilled prior to use.

All standard NMR spectra were recorded on Bruker AV I 500 or AV III 500 spectrometers, unless otherwise stated, in tubes fitted with Young's PTFE stopcocks. All ^{1}H and ^{13}C chemical shifts are reported in ppm (δ) relative to tetramethylsilane and referenced using the chemical shifts of residual protio solvent resonances (benzene, δ 7.16), unless otherwise stated. The ^{31}P $\{^1H\}$ NMR spectra were referenced to external H_3PO_4. ^{19}F NMR spectra were referenced to external $CFCl_3$.

LIFDI mass spectra were recorded on a Waters Micromass GCT Premier orthogonal time-of-flight instrument set to 1 scan per s with resolution power of 6000 FWHM and equipped with a LIFDI probe from LINDEN GmbH. Toluene was used for tuning the instrument.[66–68] The polyethylene glycol probe was kept at ambient temperature with the emitter potential at 12 kV. Activated tungsten wire LIFDI emitters (13 μm W from LINDEN) were ramped manually up to 100 mA for the emitter heating current during the experiment. The *m*/*z* values are accurate to 0.01 Da. Masses are quoted for ^{35}Cl, ^{58}Ni, ^{81}Br.

X-ray diffraction data were collected on an Oxford Diffraction SuperNova diffractometer with MoKα radiation (λ = 0.71073 Å) at 110 K unless otherwise noted. Data collection, unit cell determination and frame integration were carried out with the program CrysAlisPro.[69] Absorption corrections were applied using crystal face-indexing and the ABSPACK absorption correction software within CrysAlisPro. Structures were solved and refined using Olex2 [70] implementing SHELX algorithms. Structures were solved by either Patterson or direct methods using SHELXS-97 and refined by full-matrix least squares using SHELXL-97.[71] All non-hydrogen atoms were refined anisotropically. Carbon-bound hydrogen atoms were placed at calculated positions with fixed isotropic displacement parameters and refined using a "riding model". Detailed crystallographic data are provided in the ESI.‡

The ^{19}F-MAS NMR spectra were acquired at 9.4 T (376.48 MHz) using a Bruker Avance III HD console and a Bruker 2.5 mm H(F)/X double-resonance probe. The MAS rotors and caps were pumped under high vacuum for 24 hours then stored in the glove box where they remained for at least a week before use. A 30° tip-angle pulse was used to acquire the spectra to ensure sufficient radio frequency bandwidth to yield undistorted spinning sideband intensities. Relaxation delays of 4–7 s were used. Spectra were collected at 295 K unless stated otherwise. All shifts are reported relative to $CFCl_3$ and were calibrated using solid sodium fluoride (δ_{iso} = −224.2) as a secondary external reference. Isotropic chemical shifts were determined by comparison of three or more spectra acquired over a range of rotation frequencies (9–30 kHz). Simulation of the shielding tensors was performed using the CSA tensor module[72] within the WSolids NMR Simulation Package (Ver. 1.20.18).

Syntheses

$Ni(COD)_2$ was purchased from Sigma-Aldrich. 1,4-$C_6F_4I_2$, 1,2-$C_6F_4I_2$ (Fluorochem), Me_3SiCl and Et_3SiBr (Sigma-Aldrich) were distilled and were stored over molecular sieves. Triethylphosphine was purchased from Fluorochem. Commercially available tetramethylammonium fluoride tetrahydrate (Sigma-Aldrich) was dried following the literature method.[73,74] Complex **3F** was synthesized as previously described.[41]

^{19}F NMR aromatic resonances were assigned based on their chemical shifts and coupling constants, and ^{19}F–^{19}F COSY spectra. Note that ^{19}F nuclei *ortho* to the metal always resonate to lower field than the *meta* or *para* ^{19}F nuclei. Fluorine atoms are labelled as below:

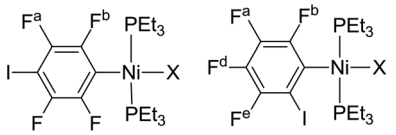

1pX **1oX**

***trans*-[NiI(2,3,5,6-C_6F_4I)(PEt_3)$_2$] (1pI).** A solution of $Ni(PEt_3)_2(COD)$ was prepared by adding PEt_3 (69 μL, 0.36 mmol) to a stirred suspension of $Ni(COD)_2$ (50 mg, 0.18 mmol) in hexane (10 mL), in a 25 mL Schlenk flask inside the glove box. The resulting mixture was stirred further to obtain a clear orange solution. A solution of 1,4-$C_6F_4I_2$ (106 mg, 0.26 mmol) was prepared separately in hexane (5 mL) in a 50 mL Schlenk flask. To this the $Ni(PEt_3)_2(COD)$ solution was added dropwise while stirring. The resulting red-brown solution was left stirring further for 15 min and then allowed to stand for 1 h upon which a red-brown solid precipitated. The solution was decanted and the residue was retained. The resulting solid was washed with cold pentane twice and dried under vacuum. Yield 105.1 mg, 84%. Single crystals for X-ray crystallographic studies were grown by layering of a saturated solution of **1pI** in THF with hexane, giving dark red crystals at the interface of the two solvents at room temperature. NMR (C_6D_6, 298 K). ^1H NMR δ 0.84 (apparent quin, J 8.0 Hz, 18H, CH_3), 1.35 (m, 12H, CH_2). $^{31}P\{^1H\}$ NMR: δ 15.4 (s). ^{19}F-NMR: δ −113.3 (AA′XX′, 2F, F^b), −124.1 (AA′XX′, 2F, F^a). Mass spectrum (LIFDI, m/z^+) 695.93 (100% M^+): anal. calcd for $C_{18}H_{30}F_4I_2NiP_2$ C, 31.02; H, 4.34; found: C, 31.12; H, 4.32.

***trans*-[NiF(2,3,5,6-C_6F_4I)(PEt_3)$_2$] (1pF).** To a THF solution (50 mL) of **1pI** (100 mg, 0.14 mmol) in a 250 mL Schlenk flask was added an excess of anhydrous tetramethylammonium fluoride (150 mg, 1.6 mmol). The solution was stirred at room temperature for 5 h giving a red-brown precipitate which was discarded. The reaction mixture was allowed to settle for 1 h and the yellow solution was decanted and passed through a short column of Celite into another Schlenk flask and the solvent was evaporated under vacuum. The residue from this evaporation was extracted with benzene as far as possible and undissolved material was allowed to settle for 30 min. The yellow solution was decanted and passed through a short column of Celite into another Schlenk flask. The solvent was evaporated under vacuum. The resulting yellow solid product was washed with cold pentane twice and dried under vacuum. Yield 60.1 mg, 71.1% yield. Single crystals of **1pF** suitable for X-ray crystallographic studies were obtained by slow diffusion of hexane into a saturated solution of **1pF** in THF/benzene at room temperature.

NMR (C_6D_6, 298 K). ^1H NMR δ 0.97 (apparent quin, J 7.7 Hz, 18H, CH_3), 1.06–1.14 (m, 12H, CH_2). $^{31}P\{^1H\}$ NMR: δ 13.1 (d, J_{PF} 46 Hz). ^{19}F NMR: δ −113.8 (AA′XX′, 2F, F^b), −123.6 (AA′XX′, 2F, F^a), −387.9 (t, J_{PF} 46 Hz, 1F, Ni–F). Mass spectrum (LIFDI, m/z^+) 587.99, (100% M^+). Anal. calcd for $C_{18}H_{30}F_5INiP_2$ C, for 36.71; H, 5.13. Found: C, 36.59; H, 5.06.

***trans*-[NiCl(2,3,5,6-C_6F_4I)(PEt_3)$_2$] (1pCl).** (a) From **1pI** and $[Me_4N]Cl$. Method as for **1pF**. Yield 55.2 mg, 63.5%. (b) From **1pF** and Me_3SiCl. Chlorotrimethylsilane (13 μL, 0.1 mmol) was added to a solution of THF (10 mL) of **1pF**, (50 mg, 0.08 mmol) and stirred for an hour. The solvent and excess reagents and by-products were removed under vacuum. The product was washed with pentane and dried. Yield 47 mg, 92%. Single crystals of **1pCl** suitable for X-ray crystallography were obtained by slow diffusion of hexane into a saturated solution of **1pCl** in THF/benzene and slow evaporation at room temperature over two weeks, yielding bright yellow blocks. NMR (C_6D_6, 298 K), ^1H NMR δ 0.89 (apparent quin, J 7.8 Hz, 18H, CH_3), 1.21–1.13 (m, 12H, CH_2). $^{31}P\{^1H\}$ NMR: δ 14.3 (s). ^{19}F NMR: δ −113.1 (AA′XX′, 2F, F^b), δ −124.1 (AA′XX′, 2F, F^a). Mass spectrum (LIFDI, m/z^+) 604.00 (100% M^+): anal. calcd for $C_{18}H_{30}ClF_4INiP_2$ C, 35.71; H, 4.99; found: C, 36.29; H, 4.87.

***trans*-[NiBr(2,3,5,6-C_6F_4I)(PEt_3)$_2$] (1pBr).** (a) From **1pI** and $[Et_4N]Br$. Method as for **1pF** except that solid was extracted with toluene instead of benzene. Yield 64.3 mg, 70.7%. (b) From **1pF** and Et_3SiBr. Bromotriethylsilane (17 μL, 0.1 mmol) was added into a solution of THF (10 mL) containing **2F** (50 mg, 0.08 mmol) and stirred for 1 h. The solvent and excess reagents and by-products were removed under vacuum. The product was washed with pentane and dried. Yield 50 mg, 90%. Single crystals of **1pBr** suitable for X-ray crystallographic studies were grown at room temperature by slow diffusion of hexane into a saturated solution of **1pBr** in benzene, yielding bright yellow blocks. NMR (C_6D_6, 298 K). ^1H: δ 0.87 (m, 18H, CH_3), 1.20–1.26 (m, 12H, CH_2). $^{31}P\{^1H\}$ NMR: δ 14.4 (s). ^{19}F NMR: δ −112.9 (AA′XX′, 2F, F^b), −123.8 (AA′XX′, 2F, F^a). Mass spectrum (LIFDI, m/z^+) 649.94 (100% M^+). Anal. calcd for $C_{18}H_{30}BrF_4INiP_2$ C, 33.27; H, 4.65. Found: C, 33.41; H, 4.56.

***trans*-[NiI(2,3,5,6-C_6F_4I)(PEt_2Ph)$_2$] (2pI).** A solution of $Ni(PEt_2Ph)_2(COD)$ was prepared by adding PEt_2Ph (62.7 μL, 0.36 mmol) to a stirred suspension of $Ni(COD)_2$ (50 mg, 0.18 mmol) in hexane (10 mL) in a 25 mL Schlenk flask inside the glove box. The resulting mixture was stirred further to obtain a clear orange solution. A solution of 1,4-$C_6F_4I_2$ (106 mg, 0.26 mmol) was prepared separately in hexane (5 mL) in a 50 mL Schlenk flask. To this solution the $Ni(PEt_2Ph)_2(COD)$ solution was added drop-wise while stirring. The resulting red-brown solution was left stirring further for 15 min and then allowed to stand for 1 h upon which a red-brown solid precipitated from the reaction mixture. The solution was decanted and the residue was retained. The resulting solid was washed with cold pentane twice and dried under vacuum. Yield 92 mg, 64%. Single crystals of **2pI** suitable for X-ray crystallographic studies

were obtained by slow diffusion of hexane into a saturated solution of **2pI** in THF/benzene yielding dark blocks. NMR (C_6D_6, 298 K), ^{1}H NMR: δ 0.85 (apparent quin, J 7.5 Hz, 12H, CH_3), 1.59 (m, 4H, CH_2), 2.03 (m, 4H, CH_2), 6.98 (broad, 6H, Ph), 7.28 (broad, 4H, Ph). ^{31}P{^{1}H} NMR: δ 16.2 (s). ^{19}F NMR: δ −114.0 (AA′XX′, 2F, F^b), −123.6 (AA′XX′, 2F, F^a). Mass spectrum (LIFDI, m/z^+) 791.90 (100%, M$^+$).

***trans*-[NiF(2,3,5,6-C$_6$F$_4$I)(PEt$_2$Ph)$_2$] (2pF).** Method as for **1pF**. Yield 55.4 mg, 64.1%. NMR (C_6D_6, 298 K). ^{1}H NMR: δ 0.92 (overlapping apparent quin, J 7.7 Hz, 12H, CH_3), 1.41 (m, 4H, CH_2), 1.72 (m, 4H, CH_2), 7.00 (broad, 6H, Ph), 7.38 (m, 4H, Ph). ^{31}P{^{1}H} NMR: δ 11.9 (d, J_{PF} 45 Hz). ^{19}F NMR: δ −115.2 (AA′XX′, 2F, F^b), −126.5 (AA′XX′, 2F, F^a), −389.7 (t, J_{PF} 45 Hz, 1F, Ni–F). Mass spectrum (LIFDI, m/z^+) 684.00 (100% M$^+$).

***trans*-[NiI(2,3,4,5-C$_6$F$_4$I)(PEt$_3$)$_2$] (1oI).** A solution of Ni(PEt$_3$)$_2$(COD) was prepared by adding PEt$_3$ (69 μL, 0.36 mmol) to a stirred suspension of Ni(COD)$_2$ (50 mg, 0.18 mmol) in hexane (10 mL) in a 25 mL Schlenk flask inside the glove box. The resulting mixture was stirred further to obtain a clear orange solution. A solution of 1,2-C$_6$F$_4$I$_2$ (106 mg, 0.26 mmol) was prepared separately in hexane (5 mL) in a 50 mL Schlenk flask. To this, the Ni(PEt$_3$)$_2$(COD) solution was added drop-wise while stirring. The resulting black-brown solution was left stirring further for 15 min. The reaction mixture was left in the freezer at −30 °C overnight for crystallization. The dark solution was decanted and the red crystals were washed with cold pentane twice and dried under vacuum. Yield 85.4 mg, 67.4%. Single crystals of **1oI(α)** were obtained overnight from a saturated hexane solution of **1oI** at −30 °C. The deep red blocks were washed with cold pentane and analysed by X-ray crystallography. Crystals grown from $CHCl_3$ layered with hexane yielded two further polymorphs, **1oI(β)** (orange blocks) and **1oI(γ)** (yellow plates). NMR (C_6D_6, 298 K). ^{1}H NMR δ 0.89 (apparent quin, J 7.8 Hz, 18H, CH_3), 1.41 (broad, 6H, CH_2), 1.51 (broad, 6H, CH_2). ^{31}P{^{1}H} NMR: δ 10.3 (s). ^{19}F NMR: δ −114.4 (dd, J_{FF} 32.0, 12.4 Hz, 1F, F^b), −115.4 (dd, J_{FF} 22.1, 12.1 Hz, 1F, F^e), −156.9 (dd, J_{FF} 31.7, 19.1 Hz, 1F, F^a), −159.1 (ddt, J_{FF} 22.19, 4 Hz, 1F, F^d). Mass spectrum (LIFDI, m/z^+) 695.90 (100%, M$^+$). Anal. calcd for $C_{18}H_{30}F_4I_2NiP_2$ C, 31.02; H, 4.34; found: C, 31.01; H, 4.22.

***trans*-[NiF(2,3,4,5-C$_6$F$_4$I)(PEt$_3$)$_2$] (1oF).** Method as for **1pF**. Yield 52 mg, 63%. Single crystals suitable for X-ray crystallography were obtained by slow diffusion of hexane into a saturated solution of **1oF** in benzene in the freezer at −30 °C over two weeks. NMR (C_6D_6, 298 K). ^{1}H NMR δ 1.00 (apparent quin, J = 7.63 Hz, 18H, CH_3), 1.10–1.2 (m, 6H, CH_2), 1.21–1.33 (m, 6H, CH_2). ^{31}P{^{1}H} NMR: δ 9.4 (d, J_{PF} 46 Hz). ^{19}F NMR: δ −115.3 (dd, J_{FF} 20, 11 Hz, 1F, F^b), −116.2 (dd, J_{FF} 31, 11 Hz, 1F, F^e), −158.2 (dd, J_{FF} 31, 19 Hz, 1F, F^d), −160.2 (apparent t, J_{FF} 19 Hz, 1F, F^a), −397.9 (td, J_{PF} 46, J_{FF} 9 Hz, 1F, Ni–F). Mass spectrum (LIFDI, m/z^+) 588.01, (100% M$^+$). Anal. calcd for $C_{18}H_{30}F_5INiP_2C$, 36.71; H, 5.13. Found: C, 36.69; H, 5.13.

***trans*-[NiCl(2,3,4,5-C$_6$F$_4$I)(PEt$_3$)$_2$] (1oCl).** (a) From **1oI** and [Me$_4$N]Cl. Method as for **1pF**. Yield 59 mg, 69% yield. Single crystals suitable for X-ray crystallography were obtained by slow diffusion of hexane into a saturated solution of **4-Cl** in THF/toluene in the freezer at −30 °C over two weeks. (b) From **1oF** and Me$_3$SiCl. Chlorotrimethylsilane (13 μL, 0.1 mmol) was added into a solution of THF (10 mL) containing **1oF** (50 mg, 0.08 mmol) and stirred for 1 h. The solvent and excess reagents and by-products were removed under vacuum. The product was washed with pentane and dried. Yield 48 mg, 93%. NMR (C_6D_6, 298 K). ^{1}H NMR δ 0.93 (apparent quin, J 7.6 Hz, 18H, CH_3), 1.24 and 1.31 (m, 12H, CH_2). ^{31}P{^{1}H} NMR: δ 9.5 (s). ^{19}F NMR: δ −114.8 (two overlapping m, 1F^e + F^b), −157.2 (dd, J_{FF} 28.7, 18.1 Hz, 1F^a), −159.5 (apparent t of m, J_{FF} 22.2, 1F^d). Mass spectrum (LIFDI, m/z^+) 603.97, (100% M$^+$). Anal. calcd for $C_{18}H_{30}ClF_4INiP_2$, C, 35.71; H, 4.99. Found: C, 36.68; H, 4.87.

Synthesis of *trans*-[NiBr(2,3,4,5-C$_6$F$_4$I)(PEt$_3$)$_2$] (1oBr). (a) From **1oI** and [Et$_4$N]Br. Method as for **1pF** but extracted with toluene instead of benzene. Yield 62 mg, 68%.

(b) From **1oF** and Et$_3$SiBr. Bromotriethylsilane (17 μL, 0.1 mmol) was added into a solution of THF (10 mL) containing **1oF**, (50 mg, 0.08 mmol) and stirred for 1 h. The solvent and excess reagents and by-products were removed under vacuum. The product was washed with pentane and dried. Yield 53 mg, 96%. NMR (C_6D_6, 298 K). ^{1}H NMR δ 0.92 (apparent quin J 7.7 Hz, 18H, CH_3), 1.30 (m, 6H, CH_2), 1.38 (m, 6H, CH_2). ^{31}P{^{1}H} NMR: δ 9.52 (s). ^{19}F NMR: δ −114.5 (dd, J_{FF} 31.2, 12.2 Hz, 1F, F^b), −115.0 (dd, J_{FF} 21.8, 11.9 Hz, 1F, F^e), −157.0 (dd, J_{FF} 32.0, 19.3 Hz, 1F, F^a), −159.3 (t of m, J_{FF} 20.8 Hz, 1F, F^d). Mass spectrum (LIFDI, m/z^+) 649.91, (100% M$^+$). Anal. calcd for $C_{18}H_{30}BrF_4INiP_2$ C, 33.27; H, 4.65. Found: C, 33.36; H, 4.54.

DFT calculations

Calculations were performed using Gaussian 09 Revision B.01.[75] Geometries optimisations were performed using BH and HLYP hybrid functional[38,76,77] with 6-31+G(d,p) for H, C, P, and F atoms and SDD effective core potentials for Ni and I. Calculation of the shielding tensors was done using BH and HLYP functional with 6-311+G(d,p) for H, C, P, F and Ni and SDD effective core potential for I. The computed tensors from Gaussian were symmetrised, diagonalised and the direction cosines visualised using either home-written Matlab scripts or the program EFGShield.[78]

Conflicts of interest

There are no conflicts of interest to declare.

Acknowledgements

We thank Dr Iain Oswald (University of Strathclyde) for determining the crystal structure of [*trans*-NiBr(PEt$_3$)$_2$]$_2$(μ-2,3,5,6-C$_6$F$_4$) and thank Professors Christopher Hunter (University of Cambridge) and Odile Eisenstein University of Montpellier for useful discussions. We acknowledge an Overseas Research Scholarship from the University of York to VT. We also acknowledge support from EPSRC (grants EP/J012955/1 and EP/J012998/1).

Notes and references

‖ The crystal structure of **1oBr** exhibited unresolved twinning and poorly resolved disorder and the geometric information was considered not of high enough quality for inclusion. Nevertheless, the major component showed the zig-zag halogen-bonded motif present in the other **1oX** structures.

** The separate crystal structure determination at 110 K (Tables 1, 2 and S6) is consistent with that presented here, determined at 111 K (Tables 3 and S15).

1 G. Cavallo, P. Metrangolo, R. Milani, T. Pilati, A. Priimagi, G. Resnati and G. Terraneo, *Chem. Rev.*, 2016, **116**, 2478–2601.
2 P. Metrangolo, H. Neukirch, T. Pilati and G. Resnati, *Acc. Chem. Res.*, 2005, **38**, 386–395.
3 A. Priimagi, G. Cavallo, P. Metrangolo and G. Resnati, *Acc. Chem. Res.*, 2013, **46**, 2686–2695.
4 T. M. Beale, M. G. Chudzinski, M. G. Sarwar and M. S. Taylor, *Chem. Soc. Rev.*, 2013, **42**, 1667–1680.
5 L. Brammer, *Faraday Discuss.*, 2017, **203**, 485–507.
6 M. Erdelyi, *Chem. Soc. Rev.*, 2012, **41**, 3547–3557.
7 M. Erdelyi, *Biochemistry*, 2017, **56**, 2759–2761.
8 L. C. Gilday, S. W. Robinson, T. A. Barendt, M. J. Langton, B. R. Mullaney and P. D. Beer, *Chem. Rev.*, 2015, **115**, 7118–7195.
9 S. H. Jungbauer and S. M. Huber, *J. Am. Chem. Soc.*, 2015, **137**, 12110–12120.
10 R. Wilcken, M. O. Zimmermann, A. Lange, A. C. Joerger and F. M. Boeckler, *J. Med. Chem.*, 2013, **56**, 1363–1388.
11 P. Auffinger, F. A. Hays, E. Westhof and P. S. Ho, *Proc. Natl. Acad. Sci. U. S. A.*, 2004, **101**, 16789–16794.
12 E. Parisini, P. Metrangolo, T. Pilati, G. Resnati and G. Terraneo, *Chem. Soc. Rev.*, 2011, **40**, 2267–2278.
13 A. R. Voth, P. Khuu, K. Oishi and P. S. Ho, *Nat. Chem.*, 2009, **1**, 74–79.
14 L. A. Hardegger, B. Kuhn, B. Spinnler, L. Anselm, R. Ecabert, M. Stihle, B. Gsell, R. Thoma, J. Diez, J. Benz, J. M. Plancher, G. Hartmann, D. W. Banner, W. Haap and F. Diederich, *Angew. Chem., Int. Ed.*, 2011, **50**, 314–318.
15 D. W. Bruce, *Struct. Bonding*, 2008, **126**, 161–180.
16 L. Brammer, G. Mínguez Espallargas and S. Libri, *CrystEngComm*, 2008, **10**, 1712–1727.
17 K. Rissanen, *CrystEngComm*, 2008, **10**, 1107–1113.
18 P. Politzer, J. S. Murray and T. Clark, *Phys. Chem. Chem. Phys.*, 2010, **12**, 7748–7757.
19 M. H. Kolar and P. Hobza, *Chem. Rev.*, 2016, **116**, 5155–5187.
20 H. Wang, W. Z. Wang and W. J. Jin, *Chem. Rev.*, 2016, **116**, 5072–5104.
21 R. D. Willett, F. Awwadi, R. Butcher, S. Haddad and B. Twamley, *Cryst. Growth Des.*, 2003, **3**, 301–311.
22 R. Bertani, P. Sgarbossa, A. Venzo, F. Lelj, M. Amati, G. Resnati, T. Pilati, P. Metrangolo and G. Terraneo, *Coord. Chem. Rev.*, 2010, **254**, 677–695.
23 F. F. Awwadi, D. Taher, S. F. Haddad and M. M. Turnbull, *Cryst. Growth Des.*, 2014, **14**, 1961–1971.
24 D. M. Ivanov, A. S. Novikov, I. V. Ananyev, Y. V. Kirina and V. Y. Kukushkin, *Chem. Commun.*, 2016, **52**, 5565–5568.
25 G. Lapadula, N. Judas, T. Friščić and W. Jones, *Chem.–Eur. J.*, 2010, **16**, 7400–7403.
26 R. W. Troff, T. Makela, F. Topic, A. Valkonen, K. Raatikainen and K. Rissanen, *Eur. J. Org. Chem.*, 2013, 1617–1637.
27 J. M. Clemente-Juan, E. Coronado, G. Mínguez Espallargas, H. Adams and L. Brammer, *CrystEngComm*, 2010, **12**, 2339–2342.
28 P. Smart, Á. Bajarano-Villafuerte and L. Brammer, *CrystEngComm*, 2013, **15**, 3151–3159.
29 J. E. Ormond-Prout, P. Smart and L. Brammer, *Cryst. Growth Des.*, 2012, **12**, 205–216.
30 F. Zordan, L. Brammer and P. Sherwood, *J. Am. Chem. Soc.*, 2005, **127**, 5979–5989.
31 M. T. Johnson, Z. Džolić, M. Cetina, O. F. Wendt, L. Öhrström and K. Rissanen, *Cryst. Growth Des.*, 2011, **12**, 362–368.
32 L. Brammer, G. Mínguez Espallargas and H. Adams, *CrystEngComm*, 2003, **5**, 343–345.
33 G. Mínguez Espallargas, L. Brammer and P. Sherwood, *Angew. Chem., Int. Ed.*, 2006, **45**, 435–440.
34 F. Zordan and L. Brammer, *Cryst. Growth Des.*, 2006, **6**, 1374–1379.
35 M. E. G. Mosquera, I. Egido, C. Hortelano, M. López-López and P. Gómez-Sal, *Faraday Discuss.*, 2017, **203**, 257–283.
36 S. Libri, N. A. Jasim, R. N. Perutz and L. Brammer, *J. Am. Chem. Soc.*, 2008, **130**, 7842–7844.
37 D. A. Smith, T. Beweries, C. Blasius, N. Jasim, R. Nazir, S. Nazir, C. C. Robertson, A. C. Whitwood, C. A. Hunter, L. Brammer and R. N. Perutz, *J. Am. Chem. Soc.*, 2015, **137**, 11820–11831.
38 T. Beweries, L. Brammer, N. A. Jasim, J. E. McGrady, R. N. Perutz and A. C. Whitwood, *J. Am. Chem. Soc.*, 2011, **133**, 14338–14348.
39 W. Sattler, S. Ruccolo and G. Parkin, *J. Am. Chem. Soc.*, 2013, **135**, 18714–18717.
40 M. Rauch, S. Ruccolo, J. P. Mester, Y. Rong and G. Parkin, *Chem. Sci.*, 2016, **7**, 142–149.
41 L. Cronin, C. L. Higgitt, R. Karch and R. N. Perutz, *Organometallics*, 1997, **16**, 4920–4928.
42 M. A. Bennett and E. Wenger, *Organometallics*, 1995, **14**, 1267–1277.
43 A. J. Edwards, A. C. Willis and E. Wenger, *Organometallics*, 2002, **21**, 1654–1661.
44 M. A. Bennett, T. W. Hambley, N. K. Roberts and G. B. Robertson, *Organometallics*, 1985, **4**, 1992–2000.
45 A. L. Keen, M. Doster and S. A. Johnson, *J. Am. Chem. Soc.*, 2007, **129**, 810–819.
46 S. Alvarez, *Dalton Trans.*, 2013, **42**, 8617–8636.
47 A. Bondi, *J. Phys. Chem.*, 1964, **68**, 441–451.
48 J. P. M. Lommerse, A. J. Stone, R. Taylor and F. H. Allen, *J. Am. Chem. Soc.*, 1996, **118**, 3108–3116.
49 E. Clot, C. Mégret, O. Eisenstein and R. N. Perutz, *J. Am. Chem. Soc.*, 2009, **131**, 7817–7827.
50 G. Mínguez Espallargas, L. Brammer, D. R. Allan, C. R. Pulham, N. Robertson and J. E. Warren, *J. Am. Chem. Soc.*, 2008, **130**, 9058–9071.

51 M. Weingarth, N. Raouafi, B. Jouvelet, L. Duma, G. Bodenhausen, K. Boujlel, B. Schollhorn and P. Tekely, *Chem. Commun.*, 2008, 5981–5983.
52 J. Viger-Gravel, S. Leclerc, I. Korobkov and D. L. Bryce, *J. Am. Chem. Soc.*, 2014, **136**, 6929–6942.
53 P. Cerreia Vioglio, M. R. Chierotti and R. Gobetto, *CrystEngComm*, 2016, **18**, 9173–9184.
54 M. R. Chierotti, A. Rossin, R. Gobetto and M. Peruzzini, *Inorg. Chem.*, 2013, **52**, 12616–12623.
55 M. C. Leclerc, J. M. Bayne, G. M. Lee, S. I. Gorelsky, M. Vasiliu, I. Korobkov, D. J. Harrison, D. A. Dixon and R. T. Baker, *J. Am. Chem. Soc.*, 2015, **137**, 16064–16073.
56 H. Saito, I. Ando and A. Ramamoorthy, *Prog. Nucl. Magn. Reson. Spectrosc.*, 2010, **57**, 181–228.
57 G. Wu, D. Rovnyak, M. J. A. Johnson, N. C. Zanetti, D. G. Musaev, K. Morokuma, R. R. Schrock, R. G. Griffin and C. C. Cummins, *J. Am. Chem. Soc.*, 1996, **118**, 10654–10655.
58 P. Garbacz, V. V. Terskikh, M. J. Ferguson, G. M. Bernard, M. Kedziorek and R. E. Wasylishen, *J. Phys. Chem. A*, 2014, **118**, 1203–1212.
59 L. J. L. Haller, E. Mas-Marza, M. K. Cybulski, R. A. Sanguramath, S. A. Macgregor, M. F. Mahon, C. Raynaud, C. A. Russell and M. K. Whittlesey, *Dalton Trans.*, 2017, **46**, 2861–2873.
60 C. M. Widdifield and R. W. Schurko, *Concepts Magn. Reson., Part A*, 2009, **34**, 91–123.
61 S. Halbert, C. Copéret, C. Raynaud and O. Eisenstein, *J. Am. Chem. Soc.*, 2016, **138**, 2261–2272.
62 F. F. Awwadi, R. D. Willett, S. F. Haddad and B. Twamley, *Cryst. Growth Des.*, 2006, **6**, 1833–1838.
63 G. Mínguez Espallargas, F. Zordan, L. Arroyo Marín, H. Adams, K. Shankland, J. van de Streek and L. Brammer, *Chem.–Eur. J.*, 2009, **15**, 7554–7568.
64 L. Brammer, E. A. Bruton and P. Sherwood, *Cryst. Growth Des.*, 2001, **1**, 277–290.
65 A. Forni, P. Metrangolo, T. Pilati and G. Resnati, *Cryst. Growth Des.*, 2004, **4**, 291–295.
66 T. A. Dransfield, R. Nazir, R. N. Perutz and A. C. Whitwood, *J. Fluorine Chem.*, 2010, **131**, 1213–1217.
67 J. H. Gross, N. Nieth, H. B. Linden, U. Blumbach, F. J. Richter, M. E. Tauchert, R. Tompers and P. Hofmann, *Anal. Bioanal. Chem.*, 2006, **386**, 52–58.
68 J. H. Gross, *J. Am. Soc. Mass Spectrom.*, 2007, **18**, 2254–2262.
69 *CrysAlisPro Version 1.171.38.46*, Rigaku Oxford Diffraction Ltd.
70 O. V. Dolomanov, L. J. Bourhis, R. J. Gildea, J. A. K. Howard and H. Puschmann, *J. Appl. Crystallogr.*, 2009, **42**, 339–341.
71 G. M. Sheldrick, *Acta Crystallogr., Sect. A: Found. Crystallogr.*, 2008, **64**, 112–122.
72 K. Eichele, R. E. Wasylishen, J. F. Corrigan, N. J. Taylor and A. J. Carty, *J. Am. Chem. Soc.*, 1995, **117**, 6961–6969.
73 K. O. Christe, W. W. Wilson, R. D. Wilson, R. Bau and J. A. Feng, *J. Am. Chem. Soc.*, 1990, **112**, 7619–7625.
74 N. A. Jasim and R. N. Perutz, *J. Am. Chem. Soc.*, 2000, **122**, 8685–8693.
75 R. B., *Gaussian 09*, Rev. B.01, see ESI.‡
76 J. Csontos, N. Y. Palermo, R. F. Murphy and S. Lovas, *J. Comput. Chem.*, 2008, **29**, 1344–1352.
77 E. Ruiz, D. R. Salahub and A. Vela, *J. Phys. Chem.*, 1996, **100**, 12265–12276.
78 S. Adiga, D. Aebi and D. L. Bryce, *Can. J. Chem.*, 2007, **85**, 496–505.